MATERIALS CHEMISTRY
FRONTIERS

RESEARCH ARTICLE

View Article Online
View Journal | View Issue

Cite this: *Mater. Chem. Front.*, 2019, **3**, 1199

Syntheses, crystal structures, chirality and aggregation-induced phosphorescence of stacked binuclear platinum(II) complexes with bridging Salen ligands†

Lang Qu, Chunbo Li, Guangyu Shen, Fei Gou, Jintong Song, Man Wang, Xuemei Xu, Xiangge Zhou and Haifeng Xiang *

Received 18th February 2019,
Accepted 17th April 2019

DOI: 10.1039/c9qm00105k

rsc.li/frontiers-materials

A novel class of cyclometalated binuclear Pt(II) complexes, [(C^N)Pt(μ-Salen)Pt(C^N)] (C^N = 2-phenylpyridine or benzo[*h*]quinoline, Salen = *N,N′*-bis(salicylidene)ethylenediamine), have been synthesized and characterized. Owing to the blockage of intramolecular rotation in the bridging Salen ligands, all the double-layer stacked complexes exhibit strong aggregation-induced phosphorescence with quantum yields up to 0.35 through well-tuned intramolecular Pt–Pt interactions (3.37–4.48 Å) and strong multiple intermolecular interactions, such as H–H, C–H, O–H, Cl–H, and Pt–H interactions. Interestingly, if chiral Salen ligands are adopted, it is facile to prepare (*R,R*)/(*S,S*) enantiopure Pt(II) complexes, which were characterized by X-ray diffraction, circular dichroism spectra and time-dependent density functional theory calculations. This is the first example of stacked binuclear Pt(II) complexes with well-known tetradentate Salen ligands as bis-bidentate-bridging ligands and would render a new structural motif for bridging ligands and chiral binuclear complexes.

Introduction

The class of cyclometalated Pt(II) complexes has been extensively investigated in the past two decades owing to their interesting and rich phosphorescence properties.[1–8] Unlike other well-known octahedral phosphorescent d^6 Ru(II)[9,10] and Ir(III)[11,12] complexes, d^8 Pt(II) complexes adopt a square-planar geometry with a vacant coordination site at the Pt(II) center, which allows axial substrate-binding interactions and might lead to strong intramolecular and intermolecular interactions consequently. Therefore, Pt(II) complexes have rich transition states including not only (π–π*) intraligand charge transfer (^{3}ILCT) and (d–π*) triplet metal-to-ligand charge transfer (^{3}MLCT) common to normal transition metal complexes, but also metal–metal-to-ligand charge transfer (^{3}MMLCT) through strong intramolecular and intermolecular Pt–Pt interactions. Moreover, strong intermolecular Pt–Pt interactions combined with intermolecular π–π stacking interactions have been widely used to promote molecular self-assembly and supramolecular gelation.[13,14] On the other hand, Pt(II) complexes are far more likely to encounter the problem of emission "aggregation-caused quenching" (ACQ),[15] because they easily form excimers through these strong intermolecular interactions in high concentrations and the solid state. In order to solve the ACQ problem, a lot of effort has been made to develop aggregation-induced emission (AIE)[15–18] or phosphorescence (AIP)[19]-active materials.

In the literature, there are a lot of phosphorescent stacked binuclear Pt(II) complexes. The cyclometalated or auxiliary ligands of these stacked binuclear Pt(II) complexes usually are C^N,[20–24] C^N^N,[25,26] N^N^N,[27–29] and C^C* (N-heterocyclic carbenes),[30,31] whose mononuclear Pt(II) complexes are highly emissive in dilute solution. The simple bidentate pyrazolate (pz),[21–25,28,31] pyridine-2-thiolate (pyt),[20] bis(diphenylphosphino)-methane (dppm),[25,26] disulfur,[29] and amidinate[30] ligands with strong coordination ability are used as bridging ligands. It has been proved that the ^{3}MMLCT transition of stacked binuclear Pt(II) complexes is strongly dependent on the intramolecular Pt–Pt distances (2.8–4.0 Å) through the interacting $5d_{z^2}$ Pt(II) orbitals.[20–31] For example, the transition energy or emission band (λ_{em}) of binuclear [(C^N)Pt(μ-pyt)Pt(C^N)] complexes can be well tuned in the whole region of visible light by the presence of steric bulk at the 3,5-positions of the bridging pz ligands, which in turn alters the Pt–Pt distance within the complex.[21,22] Our research group has a longstanding interest in the synthesis and optical properties of *N,N′*-bis(salicylidene)ethylenediamine (Salen),[32–38]

College of Chemistry, Sichuan University, Chengdu, 610041, China.
E-mail: xianghaifeng@scu.edu.cn; Fax: +86 28-8541-2291

† Electronic supplementary information (ESI) available: General, materials, computational details, crystallographic information files (CIF), crystallographic data, absorption, and fluorescence emission data. CCDC 1589703, 1589704, 1589683, 1589684, and 1589685. For ESI and crystallographic data in CIF or other electronic format see DOI: 10.1039/c9qm00105k

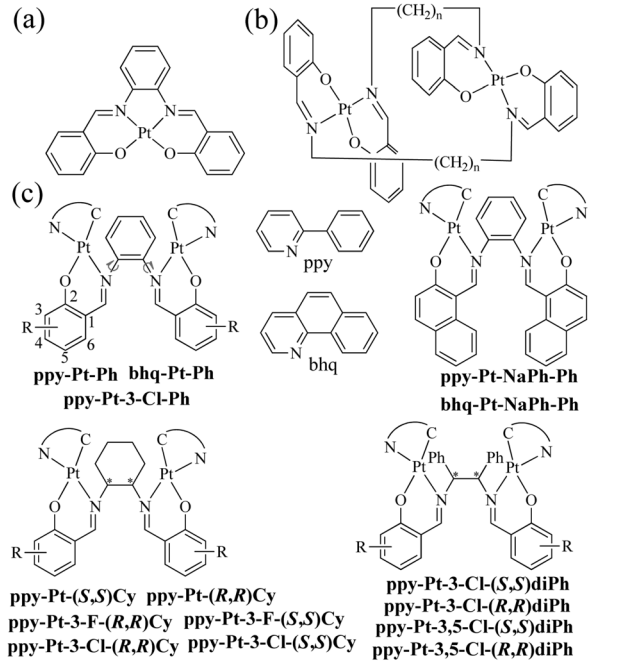

Scheme 1 Reported mononuclear Pt(Salen) complexes (a), reported binuclear $Pt_2(Salen)_2$ complexes (b), and stacked binuclear [(C^N)Pt(μ-Salen)Pt(C^N)] complexes (c) in this work.

a particular class of tetradentate N^O^O^N chelating bis-Schiff base ligands, and their complexes (Scheme 1a),[39,40] due to their facile preparation, good stabilities, biological activities, rich photophysical properties, high emission quantum yields (Φ), and wide applications in catalysts,[41,42] DNA cleavage,[43,44] optical and magnetic materials,[45,46] supramolecular materials,[47,48] cell imaging,[49,50] and organic light-emitting diodes.[51–55] When Salen ligands react with Pt^{2+} ions directly, they can act as tetradentate chelating reagents to form phosphorescent mononuclear Pt(Salen) complexes (Φ up to 0.27 in dilute MeCN) (Scheme 1a).[52–55] Moreover, Komiya *et al.*[56] reported some separate binuclear $Pt_2(Salen)_2$ complexes (Scheme 1b) which are linked by non-conjugated long heptyl and consequently exhibit AIP through intermolecular Pt–Pt interactions rather than intramolecular Pt–Pt interactions. Huang's[57] and our group[58] recently demonstrated that mononuclear [(C^N)Pt(N^O)] complexes (Φ up to 0.38 in the crystal state) and propeller-type binuclear [(C^N)Pt(μ-SA)Pt(C^N)] (SA = salicylaldehyde azine) complexes (Φ up to 0.14 in the solid state) have neither intramolecular nor intermolecular Pt–Pt interactions but show strong AIP as well. Herein we present a series of novel neutral and chiral binuclear Salen-bridged [(C^N)Pt(μ-Salen)Pt(C^N)] complexes (C^N: ppy = 2-phenylpyridine and bhq = benzo[*h*]quinolone; Salen: Ph = *N,N′*-bis(salicylidene)-1,2-phenylenediamine, Cy = *N,N′*-bis(salicylidene)-1,2-cyclohexanediamine, and diPh = *N,N′*-bis(salicylidene)-1,2-diphenylethane-1,2-diamine) (Scheme 1c). Through the blockage of the intramolecular rotation of the bridging Salen ligands and well-tuned intramolecular Pt–Pt interactions (3.37–4.48 Å), these double-layer stacked complexes exhibit strong AIP (Φ up to 0.35 in the solid state). To the best of our knowledge, they are the first examples of stacked binuclear Pt(II) complexes with well-known tetradentate Salen ligands as bis-bidentate-bridging ligands.

Results and discussion

Synthesis and characterization

All bridging Salen ligands were reasonably easy to synthesize by the condensation of a primary diamine with 2 equivalents of salicylaldehyde precursor in ethanol under reflux conditions according to our previous reports.[34,38] The reason why we chose auxiliary C^N ligands is that their Pt(II) complexes are highly phosphorescent and [(C^N)Pt(μ-Cl)$_2$Pt(C^N)] (Scheme 2) is an ideal precursor to prepare bis-cyclometalated Pt(II) complexes.[23,59] The bridging Salen ligands were adopted due to their simple, chiral, and rotatable structures (Scheme 1c) that would help to achieve chiral and AIE properties for some special applications in chiral recognition[60,61] and circularly polarized luminescence (CPL).[62,63] The binuclear Pt(II) complexes were straightforwardly synthesized according to Scheme 2. The complexes with conjugated μ-Ph are weakly soluble in CH_2Cl_2, benzene, and THF but not soluble in water, ether, ethanol, and hexane, and thus we didn't obtain their nuclear magnetic resonance (NMR) spectra. The complexes with non-conjugated μ-Cy or μ-diPh have much better solubility in CH_2Cl_2, benzene, and THF.

Absorption and AIP properties

The room-temperature UV/visible absorption and AIP properties of the Pt(II) complexes are listed in Table 1, Fig. 1–5 and Fig. S1–S12 (ESI†). These Pt(II) complexes have similar absorption spectra, even though they bear different bridging ligands and C^N auxiliary ligands. To gain insight into the nature of the excited states and transitions, density functional theory (DFT) and time-dependent-DFT (TD-DFT) calculations were carried out for **ppy-Pt-3-Cl-Ph** and **ppy-Pt-(*S*,*S*)Cy** with the Gaussian 09 program package (PBE0/SDD/6-31G).[64] The computational absorption spectra are almost identical to the experimental absorption spectra (Fig. 1 and Fig. S6, ESI†). The lower energy absorption band of **ppy-Pt-3-Cl-Ph** (λ_{abs} = 445 nm in THF) is reproduced well by the computation, which predicts one absorption band at 436 nm. The lower energy absorption is due to the highest occupied molecular orbital (HOMO) → lowest unoccupied molecular orbital (LUMO) (oscillator strength f_{OSC} = 0.0275, 91%) transition. The energy level and frontier molecular orbitals of **ppy-Pt-3-Cl-Ph** (Fig. 2) reveal that its HOMO is composed primarily of π-conjugated units of the bridging ligand (iminomethylphenol units), auxiliary ppy ligands (phenyl units), and Pt(II) ions, which might be due to their electron-donating nature.

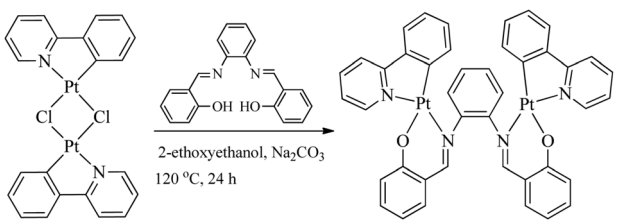

Scheme 2 Synthesis of binuclear [(C^N)Pt(μ-Salen)Pt(C^N)] complexes.

Table 1 Photophysical data of the Pt(II) complexes at room temperature. A sample without emission data means that it is non-emissive

	Medium	λ_{abs}/nm (ε/dm^3 mol^{-1} cm^{-1})	λ_{em}/nm	Stokes shift/nm	Φ	f/%
ppy-Pt-Ph	THF	333(2.00 × 10^4); 401(1.33 × 10^4)				
	THF/water	274; 403	598	195	0.001	96
	Solid		584		0.057	
ppy-Pt-3-Cl-Ph	THF	393(1.08 × 10^4); 445(5.10 × 10^3)				
	THF/water	280; 334	597	263	0.002	94
	Solid		580		0.16	
ppy-Pt-NaPh-Ph	THF	365(2.33 × 10^4) 403(1.53 × 10^4); 458(8.90 × 10^3)				
	THF/water	359	602	243	0.001	96
	Solid		604		0.017	
bhq-Pt-Ph	THF	334(2.63 × 10^4); 407(1.23 × 10^4)				
	THF/water	280; 350; 410	592	182	0.001	92
	Solid		576		0.047	
bhq-Pt-NaPh-Ph	THF	369(1.79 × 10^4); 406(1.14 × 10^4); 460(6.70 × 10^3)				
	THF/water	378	604	226	0.001	96
	Solid		605		0.047	
ppy-Pt-(*R*,*R*)Cy	THF	289(2.38 × 10^4); 372(1.33 × 10^4); 400(1.14 × 10^4)				
	THF/water	253; 297; 371; 402	569	168	0.006	96
	Solid		592		0.15	
ppy-Pt-(*S*,*S*)Cy	THF	288(3.49 × 10^4); 371(1.49 × 10^4); 399(1.28 × 10^4)				
	THF/water	253; 297; 372; 404	569	168	0.006	96
	Solid		593		0.15	
ppy-Pt-3-F-(*R*,*R*)Cy	THF	287(3.32 × 10^4); 369(1.36 × 10^4); 398(1.12 × 10^4)				
	THF/water	252; 298; 377; 402	595	194	0.010	96
	Solid		596		0.17	
ppy-Pt-3-F-(*S*,*S*)Cy	THF	287(3.45 × 10^4); 370(1.62 × 10^4); 398(1.21 × 10^4)				
	THF/water	253; 297; 378; 403	594	191	0.009	96
	Solid		597		0.18	
ppy-Pt-3-Cl-(*R*,*R*)Cy	THF	282(5.00 × 10^4); 370(2.07 × 10^4); 395(1.43 × 10^4)				
	THF/water	253; 298; 380; 402	595	193	0.016	96
	Solid		599		0.20	
ppy-Pt-3-Cl-(*S*,*S*)Cy	THF	286(3.82 × 10^4); 372(2.11 × 10^4); 398(1.40 × 10^4)				
	THF/water	252; 299; 380; 402	595	193	0.016	96
	Solid		598		0.21	
ppy-Pt-3-Cl-(*R*,*R*)diPh	THF	287(3.57 × 10^4); 377(1.56 × 10^4); 455(4.50 × 10^3)				
	THF/water	254; 299; 377; 459	595	136	0.012	96
	Solid		587		0.33	
ppy-Pt-3-Cl-(*S*,*S*)diPh	THF	288(3.22 × 10^4); 378(1.62 × 10^4); 456(4.30 × 10^3)				
	THF/water	254; 299; 378; 459	595	136	0.012	96
	Solid		586		0.35	
ppy-Pt-3,5-Cl-(*R*,*R*)diPh	THF	292(2.29 × 10^4); 376(1.81 × 10^4); 457(4.90 × 10^3)				
	THF/water	297; 381; 454	606	152	0.012	94
	Solid		610		0.21	
ppy-Pt-3,5-Cl-(*S*,*S*)diPh	THF	292(2.43 × 10^4); 375(1.83 × 10^4); 456(5.30 × 10^3)				
	THF/water	298; 380; 454	605	151	0.014	94
	Solid		607		0.20	

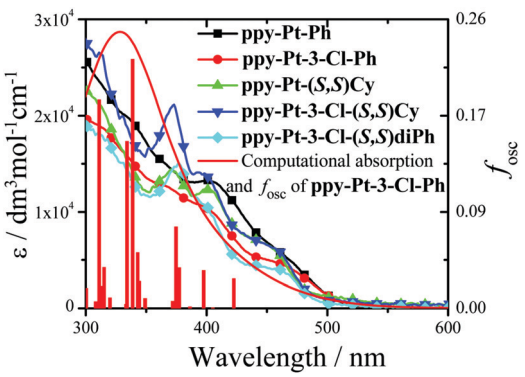

Fig. 1 Computational and experimental (in THF) absorption spectra of some Pt(II) complexes.

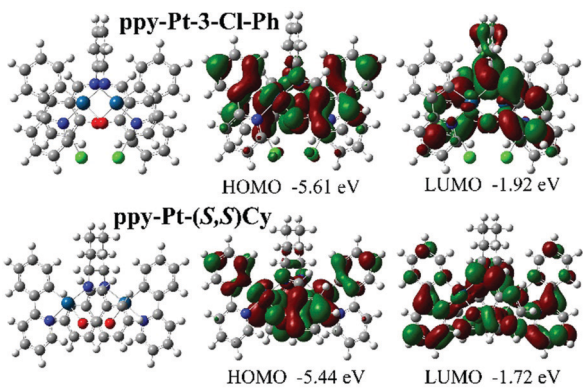

Fig. 2 Computational energy level diagram and frontier molecular orbitals of **ppy-Pt-3-Cl-Ph** and **ppy-Pt-(*S*,*S*)Cy** (in THF).

On the contrary, its LUMO is mainly made up of the whole π-functions of the bridging ligand. Therefore, the lower energy absorption can mainly be assigned to singlet intraligand charge transfer (^{1}ILCT) in the bridging ligand, ligand-to-ligand charge

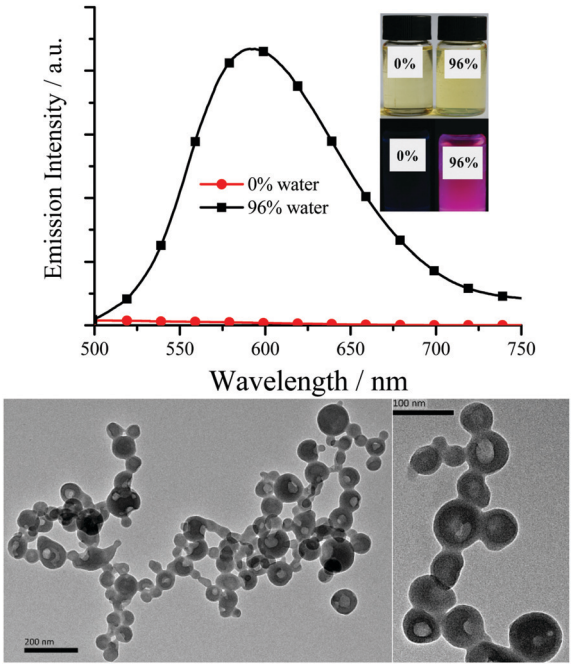

Fig. 3 Top: Emission spectra of **ppy-Pt-3-Cl-(*S,S*)Cy** in THF and THF/water (2.0×10^{-5} mol dm^{-3}). Inset: Their photographs under room light and 360 nm UV light. Bottom: Transmission electron microscopy of **ppy-Pt-3-Cl-(*S,S*)Cy** (THF/water, 96% water) on carbon-coated copper grids after solvent evaporation.

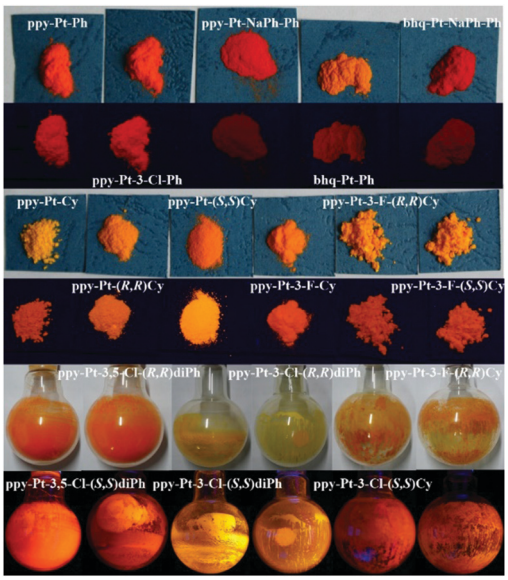

Fig. 4 Photographs of the Pt(II) complexes under room light and 360 nm UV light.

transfer (^{1}LLCT) from auxiliary ligands to the bridging ligand, and metal-to-ligand charge transfer (^{1}MLCT). The Cl atoms in the bridging ligand and pyridine rings in auxiliary ligands have little contribution to the lower energy absorption. Un-conjugated bridging **ppy-Pt-(*S,S*)Cy** shows a similar transition (423 nm, f_{OSC} = 0.0533, HOMO → LUMO, 88%) (Fig. 2 and Fig. S6, ESI†) to **ppy-Pt-3-Cl-Ph**, except that the pyridine rings and un-conjugated

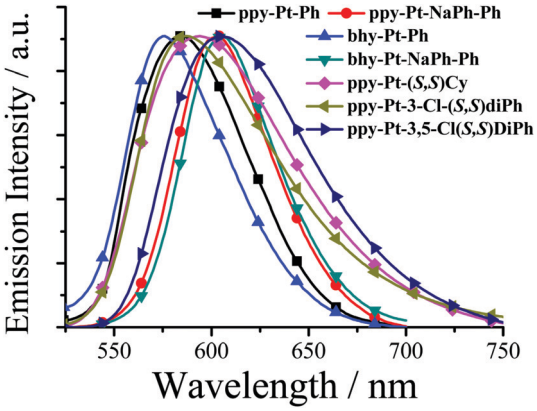

Fig. 5 Normalized emission spectra of some Pt(II) complexes in the solid state.

bridging cyclohexane have and doesn't have a contribution to the lower energy absorption, respectively.

As expected, all the Pt(II) complexes are non-emissive (Table 1) in pure dilute CH_2Cl_2, MeCN, benzene, DMSO or THF, as the intramolecular rotations (IVs) of the bridging Salen ligand provide a possible way to non-radiatively annihilate their excited states (Scheme 1c). Nonetheless, their aggregates either in THF/water or the solid state (Fig. 3–5 and Fig. S7–S11, ESI†) exhibit strong yellow–red emission (λ_{em} = 576–610 nm; Φ up to 0.35) with relative long decay lifetimes (1.68, 2.34, 1.72, and 4.02 μs for **ppy-Pt-(*R,R*)Cy**, **ppy-Pt-(*S,S*)Cy**, **ppy-Pt-3-Cl-(*R,R*)diPh**, and **ppy-Pt-3-Cl-(*S,S*)diPh**, respectively, Fig. S12, ESI†), revealing their AIP nature (water is an insoluble solvent). The absorption spectrum of **ppy-Pt-3-Cl-(*S,S*)Cy** in THF/water is similar to that in the organic solution of THF (Fig. S2, ESI†), except that there is an obvious tail in the visible region, indicating the formation of aggregated hollow nanoparticles (Fig. 3). Moreover, their absorption and excitation spectra are similar (Fig. S2, ESI†), suggesting they have a common excitation pathway, which would not be the case for a different (*e.g.*, dimer) species.

Single crystal structures

The molecular structures and arrangements play a key role in AIE.[65–68] Non-covalent interactions are also frequently involved to assist the molecules to orient and assemble. In order to enhance AIE, molecules should stack closely with not only strong non-covalent intermolecular interactions but also weak intermolecular face-to-face π–π* interactions. The former can ensure elimination of IVs; and the latter would prevent the formation of excimers. We tried many different ways to grow single crystals of these Pt(II) complexes. After dozens of attempts, we obtained suitable single crystals of **ppy-Pt-3-Cl-Ph** (CCDC: 1589703), **ppy-Pt-NaPh-Ph** (CCDC: 1589704), racemic **ppy-Pt-Cy** (CCDC: 1589683), **ppy-Pt-(*S,S*)Cy** (CCDC: 1589684), and **ppy-Pt-(*R,R*)Cy** (CCDC: 1589685) for X-ray structure determination by slow diffusion/evaporation of a CH_2Cl_2/hexane or $CHCl_3$/hexane solution.† The X-ray single crystals of racemic **ppy-Pt-Cy** were obtained from a mixture of enantiopure complexes (1 : 1) in solution. In general, strong intermolecular interactions in the crystal are in the range

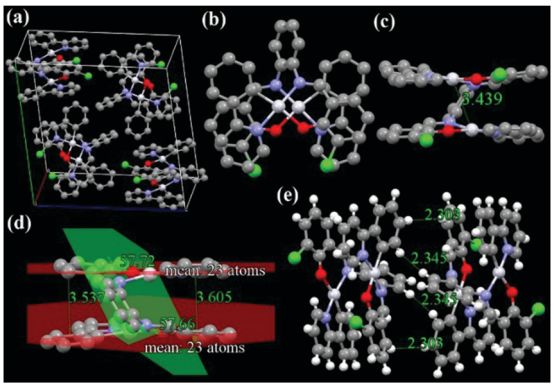

Fig. 6 X-ray single crystal structures and packing of **ppy-Pt-3-Cl-Ph** molecules (a: molecule packing in one crystal cell; b: top view; c and d: side view; e: intermolecular interactions of the two closest molecules). H atoms are omitted in a–d.

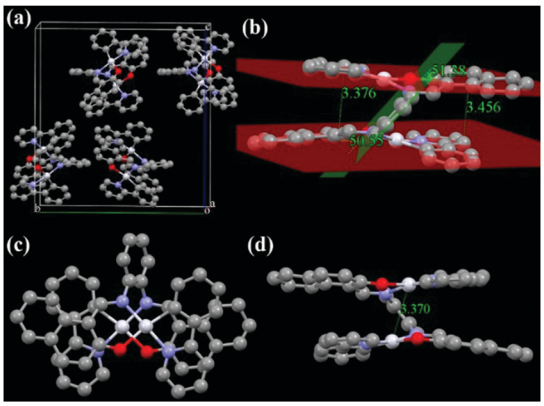

Fig. 7 X-ray single crystal structures and packing of **ppy-Pt-NaPh-Ph** molecules (a: molecule packing in one crystal cell; b and d: side view; c: top view). H atoms and $CHCl_3$ solvent molecules are omitted.

1.9–2.3 Å and 2.2–3.0 Å for hydrogen bonds and non-hydrogen bonds, respectively.[18,36,38,58,63,69]

The X-ray single-crystal structures and arrangements of **ppy-Pt-3-Cl-Ph** are shown in Fig. 6 and Fig. S13 (ESI†). **ppy-Pt-3-Cl-Ph** molecules are stacked to exhibit lamellar packing with a distance of 7.092 Å. Unlike the square-planar mononuclear Pt(Salen) complexes (Scheme 1a), the I-type binuclear **ppy-Pt-3-Cl-Ph** complex bears two planes of Pt(II) coordination systems that are linked by a central bridge of a benzene ring. The four coordination atoms of C^N^O^N and central Pt^{II} are almost located in one plane and the Pt–N, Pt–O, and Pt–C bonds are of similar lengths (2.006–2.068 Å) to what was found in normal Pt(Salen) complexes,[54] which indicates that the **ppy-Pt-3-Cl-Ph** complex has a suitable square-planar coordination environment for chelating the Pt^{II} cation. Since the dihedral angle between these two Pt(II) coordination systems and the central benzene bridge is 57.72° and 57.66°, respectively, the two Pt(II) coordination systems are almost parallel with an interplanar distance (*d*) of 3.537–3.605 Å, which reveals that there are some weak intramolecular π–π stacking interactions in the **ppy-Pt-3-Cl-Ph** complex. Some modest intramolecular Pt^{II}–Pt^{II} interactions (3.439 Å) are observed as well. Due to its staggered arrangement, there are no strong intermolecular π–π stacking interactions and Pt^{II}–Pt^{II} interactions (7.390 Å) between two neighboring **ppy-Pt-3-Cl-Ph** molecules, which would be beneficial in preventing the formation of excimers. On the other hand, many strong intermolecular noncovalent interactions including not only normal H–H (2.303–2.851 Å), C–H (2.793–2.797 Å), and O–H (2.650 Å) but also Cl–H (2.911 Å, halogen bonds) exist between the two neighboring **ppy-Pt-3-Cl-Ph** molecules. These strong intermolecular interactions could restrict the IVs of the bridging ligand, and thus the phosphorescence is enhanced finally.

With π-extended conjugation in the bridging ligand, **ppy-Pt-NaPh-Ph** molecules (Fig. 7 and Fig. S14, ESI†) exhibit a similar lamellar packing to **ppy-Pt-3-Cl-Ph** molecules. The dihedral angle between the two Pt(II) coordination systems and the central benzene bridge is 51.38° and 50.55°, respectively. Their interplanar distances are in the range of 3.376–3.456 Å, indicating that intramolecular π–π stacking interactions in **ppy-Pt-NaPh-Ph** are stronger than those in **ppy-Pt-3-Cl-Ph**. Moreover, stronger intramolecular Pt^{II}–Pt^{II} interactions (3.370 Å) and weaker intermolecular H–H (2.430–2.945 Å) and C–H (2.842 Å) interactions are observed for **ppy-Pt-NaPh-Ph** molecules. All the above factors lead to solid-state **ppy-Pt-NaPh-Ph** (λ_{em} = 605 nm; Φ = 0.017) emitting red-shifted emission along with a much lower Φ than solid-state **ppy-Pt-3-Cl-Ph** (λ_{em} = 580 nm; Φ = 0.16).

Linked with an un-conjugated Cy ligand, **ppy-Pt-(*S*,*S*)Cy** and **ppy-Pt-(*R*,*R*)Cy** molecules (Fig. 8 and Fig. S15, ESI†) exhibit lamellar packing as well. The molecular structures and arrangements of the **ppy-Pt-(*S*,*S*)Cy** and **ppy-Pt-(*R*,*R*)Cy** enantiomers are similar and mirrored, which might contribute to their similar

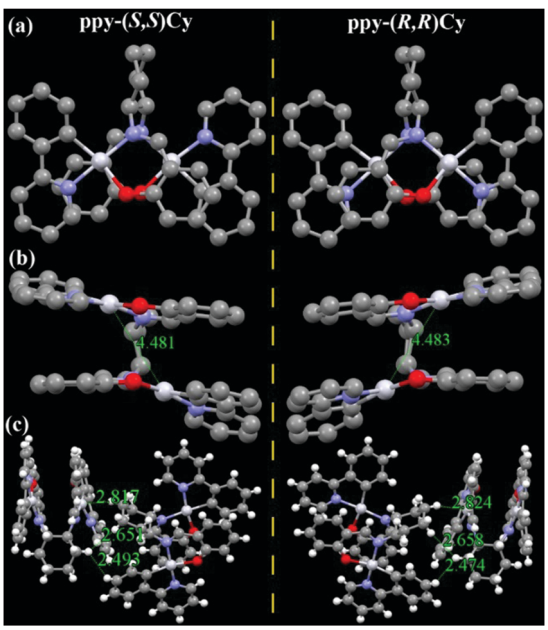

Fig. 8 X-ray single crystal structures and packing of **ppy-Pt-(*S*,*S*)Cy** and **ppy-Pt-(*R*,*R*)Cy** molecules (a: top view; b: side view; c: intermolecular interactions of the two neighboring molecules). Some H atoms and CH_2Cl_2 solvent molecules are omitted.

absorption and AIP properties.[38,63,69] In this section, **ppy-Pt-(*S,S*)Cy** was discussed as an example. Since the un-conjugated Cy bridging ligand is flexible, the two Pt(II) coordination systems are not parallel with a dihedral angle of 14.12°. There are no intramolecular π–π stacking interactions and Pt^{II}–Pt^{II} interactions (4.481 Å) in one **ppy-Pt-(*S,S*)Cy** molecule. For two neighboring **ppy-Pt-(*S,S*)Cy** molecules, however, not only some strong intermolecular H–H (2.353–2.692 Å) and C–H (2.875 Å) interactions but also strong Pt–H (2.817 Å) interactions are observed. Therefore, solid-state **ppy-Pt-(*S,S*)Cy** (λ_{em} = 593 nm; Φ = 0.15) has a high Φ.

Racemic **ppy-Pt-Cy** (Fig. 9 and Fig. S16, ESI†) has a totally different molecular arrangement from enantiopure **ppy-Pt-(*S,S*)Cy** and **ppy-Pt-(*R,R*)Cy**, even though they have similar AIP properties. In the single crystals of **ppy-Pt-Cy**, one pair of (*S,S*) and (*R,R*) enantiomers (1 : 1) was found, and thus these (*R*)/(*S*)-chirality-induced interactions[38,63] between the two enantiomers would help **ppy-Pt-Cy** molecules arrange in herringbone packing. Similar strong intermolecular H–H (2.390–2.876 Å), C–H (2.825 Å), and Pt–H (2.881 Å) interactions are observed in two neighboring **ppy-Pt-Cy** molecules. We failed to grow single crystals of the complexes bearing diPh bridging ligands. Our previous work[38] reveals that diPh ligands have a 1,2-diphenylethane bridge but not a circular bridge of cyclohexane; hence, diPh ligands are more flexible than Cy ligands. We speculate that, compared with Cy-linked complexes, diPh-linked complexes would be more flexible as well and consequently pack more closely to enhance AIP. The Φ of solid-state **ppy-Pt-3-Cl-(*S,S*)diPh** is up to 0.35, which is unexpected for binuclear Pt(II) complexes[70] and even higher than that of mononuclear Pt(Salen) complexes (Φ up to 0.27 in dilute MeCN).[54] The presence of Cl and F atoms would aid in AIP through intermolecular halogen bonds (Fig. S13, ESI†).[36–38]

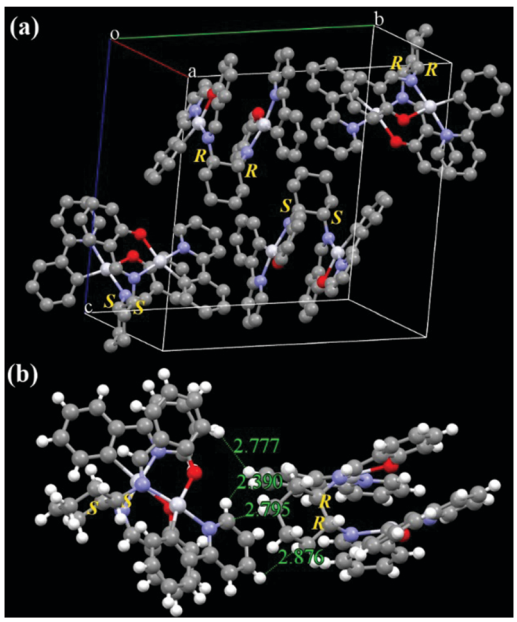

Fig. 9 X-ray single crystal structures and packing of racemic **ppy-Pt-Cy** molecules (a: molecule packing in one crystal cell; b: intermolecular interactions of the two neighboring molecules). Some H atoms are omitted.

It is interesting that similar cyclometallated [(ppy)Pt(pop)] (pop = 2-(5-phenyl-1,3,4-oxadiazol-2-yl)phenol) Pt(II) complexes[71] are known to be emissive in solution. However, some similar cyclometallated [(C^N)Pt(N^O)] complexes[57] and [(C^N)Pt(μ-SA)-Pt(C^N)] complexes[58] show strong AIP as well. This might be caused by the differences of their chemical and electronic structures.

Chirality properties

The un-conjugated Pt(II) complexes with Cy and diPh bridging ligands have two (*S,S*) or (*R,R*) chiral carbons and might be used in some special applications of enantioselective catalysis,[42] chiral recognition,[60,61] and CPL,[62,63] and thus their chirality properties were studied by circular dichroism (CD) spectra and TD-DFT calculations (Fig. 10). As example, racemic **ppy-Pt-Cy** has no CD signals in dilute MeCN. Enantiopure **ppy-Pt-(*S,S*)Cy** exhibits three positive Cotton peaks at 390, 353, and 255 nm and two negative Cotton peaks at 448 and 300 nm. On the other hand, enantiopure **ppy-Pt-(*R,R*)Cy** shows exactly the mirror CD spectrum with two positive Cotton peaks at 488 and 300 nm and three negative Cotton peaks at 391, 352, and 255 nm, indicating the fact that **ppy-Pt-(*S,S*)Cy** and **ppy-Pt-(*R,R*)Cy** are a pair of enantiomers. The calculated CD spectrum of **ppy-Pt-(*S,S*)Cy** fits well with the experimental CD spectrum (Fig. 10), which further confirms its (*S,S*) chirality. **ppy-Pt-3-F-(*S,S*)Cy**, **ppy-Pt-3-F(*R,R*)Cy**, **ppy-Pt-3-Cl-(*S,S*)diPh**, and **ppy-Pt-3-Cl-(*R,R*)diPh** have similar chirality properties to **ppy-Pt-(*S,S*)Cy** and **ppy-Pt-(*R,R*)Cy**, which is consistent with their similar conjugation and chiral carbons. Our previous work[38] demonstrated that the free bridging Cy and diPh ligands have identical CD signals to the corresponding complexes at high energy (<370 nm), and thus the high-energy CD signals can be assigned to the chiral bridging Salen ligands themselves (^{1}ILCT) and the lower-energy CD signals (>370 nm) can be mainly assigned to ^{1}LLCT and ^{1}MLCT.

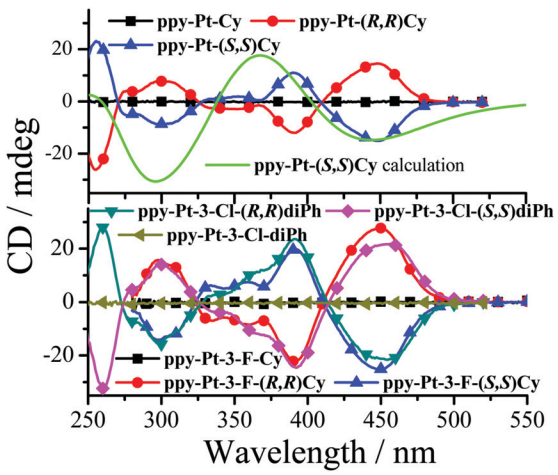

Fig. 10 Experimental CD spectra of **ppy-Pt-(*S,S*)Cy**, **ppy-Pt-(*R,R*)Cy**, racemic **ppy-Pt-cy**, **ppy-Pt-3-F-(*S,S*)Cy**, **ppy-Pt-3-F(*R,R*)Cy**, racemic **ppy-Pt-3-F-Cy**, **ppy-Pt-3-Cl-(*S,S*)diPh**, **ppy-Pt-3-Cl-(*R,R*)diPh**, and racemic **ppy-Pt-3-Cl-diPh** (5.0×10^{-5} mol dm^{-3} in MeCN). Computational CD spectra of **ppy-Pt-(*S,S*)Cy** (in THF).

Luminescence mechanism

DFT was used to calculate optimized singlet- and triplet-state structures of gas-state **ppy-Pt-(*S,S*)Cy**. As shown in Fig. 11, in the gas state or dilute solution, the optimized singlet- and triplet-state structures of **ppy-Pt-(*S,S*)Cy** are different from its single-crystal structure, which would indicate that the C–N single bonds of the bridging Salen ligand (Scheme 1c) may be rotatable and provide a possible way to non-radiatively annihilate the excited states consequently.[63] The time-resolved emission spectra (Fig. S12, ESI†) reveal that the Pt(II) complexes only have one type of emission decay lifetime in the region of 1.68–4.02 μs. This indicates that the emission may be either phosphorescence or delayed fluorescence. For metal–organic complexes, delayed fluorescence is often observed for Cu(I), Ag(I) Au(I), and Sn(IV) complexes.[72,73] For Pt(II) complexes, the emission is often phosphorescence rather than delayed fluorescence.[1–8] Moreover, we used DFT to calculate the singlet–triplet energy gap ΔE_{ST}, defined as the gap between the lowest energy triplet state (T_1) and the lowest energy singlet state (S_1). When ΔE_{ST} is sufficiently small, taken usually as <0.1 eV, the upconversion from the triplet state to the singlet state by reverse intersystem-crossing becomes possible.[74] The ΔE_{ST} of **ppy-Pt-(*S,S*)Cy** is 0.27 eV, which is much bigger than 0.1 eV. Therefore, the emission of Pt(II) complexes is phosphorescence rather than delayed fluorescence.

It is surprising that the quantum yield (around 0.01) of Pt(II) complexes in the THF/water mixture is quite low. The solid powders of **ppy-Pt-(*S,S*)Cy** have intense and sharp X-ray powder diffraction peaks (Fig. S17, ESI†), which indicate that the solid powders are mainly microcrystalline and the emission might be caused by the aggregated crystallites. However, the cast film of **ppy-Pt-3-F-(*S,S*)Cy**-doped poly(methyl methacrylate) (PMMA) emits strong emission as well, revealing that the amorphous and aggregated Pt(II) complex in PMMA is emissive (Fig. S18, ESI†). Therefore, the low quantum yield in the THF/water mixture might be caused by self-assembly (Fig. 3). Of course, we can't exclude the possibility of crystallization-induced emission.

Experimental

Materials and instrumentation

All reagents were purchased from commercial suppliers and used without further purification. All commercial chemicals were used without further purification unless otherwise stated. UV/visible absorption spectra were recorded using a UV 765 spectrophotometer with quartz cuvettes of 1 cm pathlength. Fluorescence spectra were obtained using an F-7000 fluorescence spectrophotometer (Hitachi) at room temperature. The slit width was 5.0 nm for both excitation and emission. The photon multiplier voltage was 700 V. Fluorescence lifetime data were determined in a 1 mm cell on a Hamamatsu FL920S instrument. The single-crystals were obtained by slow diffusion/evaporation of a CH_2Cl_2/$CHCl_3$/hexane solution at room temperature during about one week.

^{1}H and ^{13}C NMR spectra were recorded on a Brüker Advance 400 spectrometer (^{1}H: 400 MHz, ^{13}C: 101 MHz). Chemical shifts (δ) for ^{1}H and ^{13}C NMR spectra are given in ppm relative to TMS. The residual solvent signals were used as references for ^{1}H and ^{13}C NMR spectra and the chemical shifts converted to the TMS scale ($CDCl_3$: $\delta_H = 7.26$ ppm, $\delta_C = 77.16$ ppm). HR-MS were obtained with a Waters-Q-TOF-Premier (electrospray ionization mass spectrometry, ESI). X-Ray single-crystal diffraction data were collected on an Oxford Xcalibur E CCD area-detector diffractometer.

Measurement of fluorescence quantum yield (Φ)

The quantum yield of a solution sample was measured by the optically dilute method of Demas and Crosby with a standard of quinine sulfate ($\Phi_r = 0.55$, quinine in 0.05 mol dm^{-3} sulfuric acid) calculated by: $\Phi_s = \Phi_r(B_r/B_s)(n_s/n_r)^2(D_s/D_r)$, where the subscripts s and r refer to the sample and reference standard solution respectively; n is the refractive index of the solvents; and D is the integrated intensity. The excitation intensity B is calculated by: $B = 1 - 10^{-AL}$, where A is the absorbance at the excitation wavelength and L is the optical path length ($L = 1$ cm in all cases). The refractive indices of the solvents at room temperature are taken from standard sources. Errors for the Φ values (±10%) are estimated. The quantum yield of a solid sample was measured by an integrating sphere.

Computational details

The program Gaussian 09 was employed to perform DFT and TD-DFT calculations based on the X-ray single-crystal structure of the Pt(II) complexes. The ground state geometry was optimized using DFT and excited states were predicted using the ground state geometry using TD-DFT, from which UV/vis absorption and CD spectra were predicted. Calculations were run at the PBE0/SDD/6-31G level (pcm method; 50 singlet–singlet transitions).[64]

General procedure for the preparation of the Pt(II) complexes

Bridging ligands were synthesized according to our previous work.[38] The Pt(II) complexes were synthesized according to a procedure modified from that reported in the literature.[58] Pt(II) dichloro-bridged dimers were synthesized from the starting materials of K_2PtCl_4 and 2-phenylpyridine according to a previous report.[59] A solution of Pt(II) dichloro-bridged dimers, 0.5 equiv. of the bridging ligand and 5 equiv. of Na_2CO_3 in 2-ethoxyethanol was heated to reflux for 24 h under a N_2 atmosphere. Then the reaction mixture was concentrated under reduced pressure. A few milliliters of dichloromethane was added gradually to give the

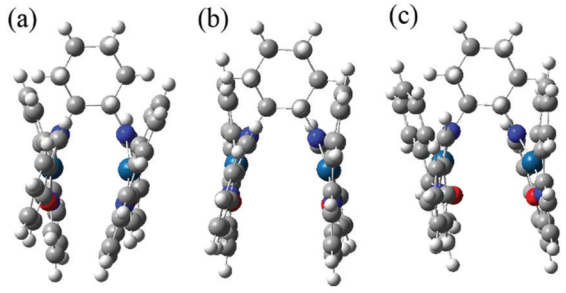

Fig. 11 Single-crystal structure (a) and optimized singlet- (b) and triplet-state (c) structures of gas-state **ppy-Pt-(*S,S*)Cy**.

crude product, which was purified by silica gel column chromatography using dichloromethane as the eluent to give pure products with moderate yields (10–28%).

ppy-Pt-Ph. (12% yield); HPLC *m*/*z* 1034.1566 [[M + Na]$^+$] (calcd *m*/*z* 1034.1541).

ppy-Pt-3-Cl-Ph. (15% yield); HPLC *m*/*z* 1102.0755 [[M + Na]$^+$] (calcd *m*/*z* 1102.0761).

ppy-Pt-NaPh-Ph. (10% yield); HPLC *m*/*z* 11134.1854 [[M + Na]$^+$] (calcd *m*/*z* 1134.1841).

bhq-Pt-Ph. (11% yield); HPLC *m*/*z* 1082.1566 [[M + Na]$^+$] (calcd *m*/*z* 1082.1541).

bhq-Pt-NaPh-Ph. (10% yield); HPLC *m*/*z* 1182.1883 [[M + Na]$^+$] (calcd *m*/*z* 1182.1854).

ppy-Pt-(*R*,*R*)Cy. (25% yield); ^{1}H NMR (400 MHz, $CDCl_3$, δ): 9.14 (s, 2H), 8.14 (s, 2H), 7.66 (t, 2H), 7.40 (d, 2H), 7.33 (s, 2H), 7.13 (s, 2H), 7.00 (dd, 8H), 6.81 (d, 2H), 6.59 (d, 2H), 6.07 (t, 2H), 4.95 (d, 2H), 2.60 (d, 2H), 1.94 (s, 4H), 1.57 (s, 2H); ^{13}C NMR (101 MHz, $CDCl_3$, δ): 167.13, 165.16, 160.28, 146.51, 146.03, 143.54, 137.54, 134.09, 133.98, 133.51, 129.19, 123.10, 122.87, 122.22, 121.58, 120.36, 117.61, 113.81, 75.22, 33.95, 24.83; HPLC *m*/*z* 1041.2037 [[M + Na]$^+$] (calcd *m*/*z* 1041.2031).

ppy-Pt-(*S*,*S*)Cy. (27% yield); ^{1}H NMR (400 MHz, $CDCl_3$, δ): 9.14 (s, 2H), 8.14 (s, 2H), 7.66 (t, 2H), 7.40 (d, 2H), 7.33 (s, 2H), 7.13 (s, 2H), 7.00 (dd, 8H), 6.81 (d, 2H), 6.59 (d, 2H), 6.07 (t, 2H), 4.95 (d, 2H), 2.60 (d, 2H), 1.94 (s, 4H), 1.57 (s, 2H); ^{13}C NMR (101 MHz, $CDCl_3$, δ): 167.13, 165.16, 160.28, 146.51, 146.03, 143.54, 137.54, 134.09, 133.98, 133.51, 129.19, 123.10, 122.87, 122.22, 121.58, 120.36, 117.61, 113.81, 75.22, 33.95, 24.83; HPLC *m*/*z* 1041.2037 [[M + Na]$^+$] (calcd *m*/*z* 1041.2031).

ppy-Pt-3-F-(*R*,*R*)Cy. (28% yield); ^{1}H NMR (400 MHz, $CDCl_3$, δ): 9.23 (dd, 2H), 7.94 (d, 2H), 7.67 (td, 2H), 7.36–7.28 (m, 4H), 7.19–7.09 (m, 4H), 7.08–6.98 (m, 4H), 6.71 (ddd, 2H), 6.54 (d, *J* = 8.0 Hz, 2H), 5.97 (td, 2H), 4.96 (d, 2H), 2.53 (d, 2H), 2.00 (d, 4H), 1.60 (s, 2H); ^{13}C NMR (101 MHz, $CDCl_3$, δ): 166.76, 159.61, 159.58, 155.63, 154.29, 154.15, 153.22, 146.73, 146.15, 143.09, 137.51, 133.86, 129.13, 128.39, 128.35, 124.88, 124.83, 122.97, 122.29, 120.73, 117.48, 117.38, 117.30, 111.99, 111.92, 76.07, 32.86, 24.69; HPLC *m*/*z* 1077.8883 [[M + Na]$^+$] (calcd *m*/*z* 1077.8875).

ppy-Pt-3-F-(*S*,*S*)Cy. (26% yield); ^{1}H NMR (400 MHz, $CDCl_3$, δ): 9.23 (dd, 2H), 7.94 (d, 2H), 7.67 (td, 2H), 7.36–7.28 (m, 4H), 7.19–7.09 (m, 4H), 7.08–6.98 (m, 4H), 6.71 (ddd, 2H), 6.54 (d, 2H), 5.97 (td, 2H), 4.96 (d, 2H), 2.53 (d, 2H), 2.00 (d, 4H), 1.60 (s, 2H); ^{13}C NMR (101 MHz, $CDCl_3$, δ): 166.76, 159.61, 159.58, 155.63, 154.29, 154.15, 153.22, 146.73, 146.15, 143.09, 137.51, 133.86, 129.13, 128.39, 128.35, 124.88, 124.83, 122.97, 122.29, 120.73, 117.48, 117.38, 117.30, 111.99, 111.92, 76.07, 32.86, 24.69; HPLC *m*/*z* 1077.8883 [[M + Na]$^+$] (calcd *m*/*z* 1077.8875).

ppy-Pt-3-Cl-(*R*,*R*)Cy. (24% yield); ^{1}H NMR (400 MHz, $CDCl_3$, δ): 9.35 (s, 2H), 7.95 (s, 2H), 7.67 (td, 2H), 7.33 (dd, 4H), 7.23–6.88 (m, 10H), 6.68 (dd, 2H), 5.98 (t, 2H), 4.95 (d, 2H), 2.53 (d, 2H), 2.02 (d, 4H), 1.61 (t, 2H); ^{13}C NMR (101 MHz, $CDCl_3$, δ): 166.50, 160.24, 159.26, 147.28, 146.33, 143.18, 137.43, 133.88, 132.89, 132.18, 129.09, 125.57, 123.68, 122.98, 122.22, 120.83, 117.27, 113.39, 76.18, 33.05, 24.46; HPLC *m*/*z* 1109.1252 [[M + Na]$^+$] (calcd *m*/*z* 1109.1249).

ppy-Pt-3-Cl-(*S*,*S*)Cy. (22% yield); ^{1}H NMR (400 MHz, $CDCl_3$, δ): 9.35 (s, 2H), 7.95 (s, 2H), 7.67 (td, 2H), 7.33 (dd, 4H), 7.23–6.88 (m, 10H), 6.68 (dd, 2H), 5.98 (t, 2H), 4.95 (d, 2H), 2.53 (d, 2H), 2.02 (d, 4H), 1.61 (t, 2H); ^{13}C NMR (101 MHz, $CDCl_3$, δ): 166.50, 160.24, 159.26, 147.28, 146.33, 143.18, 137.43, 133.88, 132.89, 132.18, 129.09, 125.57, 123.68, 122.98, 122.22, 120.83, 117.27, 113.39, 76.18, 33.05, 24.46; HPLC *m*/*z* 1109.1252 [[M + Na]$^+$] (calcd *m*/*z* 1109.1249).

ppy-Pt-3-Cl-(*R*,*R*)diPh. (13% yield); ^{1}H NMR (400 MHz, $CDCl_3$, δ): 9.45 (d, 2H), 7.78–7.66 (m, 4H), 7.56–7.45 (m, 6H), 7.37–7.27 (m, 8H), 7.23–7.19 (m, 2H), 7.13 (ddd, 8H), 7.00 (d, 2H), 6.25 (dd, 2H), 5.95 (t, 2H); ^{13}C NMR (101 MHz, $CDCl_3$, δ): 166.43, 165.06, 158.99, 147.11, 146.92, 140.93, 140.41, 137.57, 133.05, 132.80, 132.00, 129.24, 128.84, 128.51, 128.08, 125.37, 123.42, 122.59, 120.62, 117.51, 113.27, 73.08; HPLC *m*/*z* 1207.1412 [[M + Na]$^+$] (calcd *m*/*z* 1207.1408).

ppy-Pt-3-Cl-(*S*,*S*)diPh. (15% yield); ^{1}H NMR (400 MHz, $CDCl_3$, δ): 9.45 (d, 2H), 7.78–7.66 (m, 4H), 7.56–7.45 (m, 6H), 7.37–7.27 (m, 8H), 7.23–7.19 (m, 2H), 7.13 (ddd, 8H), 7.00 (d, 2H), 6.25 (dd, 2H), 5.95 (t, 2H); ^{13}C NMR (101 MHz, $CDCl_3$, δ): 166.43, 165.06, 158.99, 147.11, 146.92, 140.93, 140.41, 137.57, 133.05, 132.80, 132.00, 129.24, 128.84, 128.51, 128.08, 125.37, 123.42, 122.59, 120.62, 117.51, 113.27, 73.08; HPLC *m*/*z* 1207.1412 [[M + Na]$^+$] (calcd *m*/*z* 1207.1408).

ppy-Pt-3,5-Cl-(*R*,*R*)diPh. (13% yield); ^{1}H NMR (400 MHz, $CDCl_3$, δ): 9.37 (d, 2H), 7.78–7.70 (m, 4H), 7.40 (ddd, 16H), 7.13 (ddd, 8H), 7.02 (d, 2H), 6.17 (d, 2H); ^{13}C NMR (101 MHz, $CDCl_3$, δ): 166.00, 164.58, 157.50, 146.98, 146.64, 140.15, 137.89, 132.60, 131.91, 131.01, 129.10, 129.00, 128.85, 128.30, 126.27, 123.53, 123.33, 123.19, 120.60, 117.58, 116.77, 72.91; HPLC *m*/*z* 1275.0639 [[M + Na]$^+$] (calcd *m*/*z* 1275.0629).

ppy-Pt-3,5-Cl-(*S*,*S*)diPh. (13% yield); ^{1}H NMR (400 MHz, $CDCl_3$, δ): 9.37 (d, 2H), 7.78–7.70 (m, 4H), 7.40 (ddd, 16H), 7.13 (ddd, 8H), 7.02 (d, 2H), 6.17 (d, 2H); ^{13}C NMR (101 MHz, $CDCl_3$, δ): 166.00, 164.58, 157.50, 146.98, 146.64, 140.15, 137.89, 132.60, 131.91, 131.01, 129.10, 129.00, 128.85, 128.30, 126.27, 123.53, 123.33, 123.19, 120.60, 117.58, 116.77, 72.91; HPLC *m*/*z* 1275.0639 [[M + Na]$^+$] (calcd *m*/*z* 1275.0629).

Conclusions

In summary, we have developed a straightforward way to prepare a new class of binuclear cyclometalated Pt(II) complexes with well-known tetradentate Salen ligands as bridging ligands. These double-layer stacked complexes exhibit strong AIP through well-tuned intramolecular Pt–Pt interactions and strong multiple intermolecular interactions, such as H–H, C–H, O–H, Cl–H, and Pt–H interactions. Furthermore, chirality can be facile to introduce by the presence of chiral (*S*,*S*) and (*R*,*R*) cyclohexane and 1,2-diphenylethane in the bridging Salen ligands, which might provide a new paradigm in the design of AIP active dyes for developing phosphorescent materials, enantioselective catalysis, chiral recognition, CPL, and so on.

Conflicts of interest

There are no conflicts to declare.

Acknowledgements

This work was supported by the National Natural Science Foundation of China (no. 21871192) and Sichuan Science and Technology Program (no. 2018JY0559). We acknowledge the comprehensive training platform of the specialized laboratory of the College of Chemistry, Sichuan University, for material analysis. We would like to thank the Analytical & Testing Center of Sichuan University for CCD X-ray single crystal diffractometer work and circular dichroism CD spectrometer work. We are grateful to Daibing Luo and Yani Xie for help with the single crystal and circular dichroism measurements.

Notes and references

1 C. W. Chan, L. K. Cheng and C. M. Che, *Coord. Chem. Rev.*, 1994, **132**, 87–97.
2 F. N. Castellano, I. E. Pomestchenko, E. Shikhova, F. Hua, M. L. Muro and N. Rajapakse, *Coord. Chem. Rev.*, 2006, **250**, 1819–1828.
3 J. A. G. Williams, *Top. Curr. Chem.*, 2007, **281**, 205–268.
4 J. A. G. Williams, S. Develay, D. L. Rochester and L. Murphy, *Coord. Chem. Rev.*, 2008, **252**, 2596–2611.
5 L. Murphy and J. A. G. Williams, *Top. Organomet. Chem.*, 2010, **28**, 75–111.
6 Y. Feng, J. H. Cheng, L. Zhou, X. G. Zhou and H. F. Xiang, *Analyst*, 2012, **137**, 4885–4901.
7 H. F. Xiang, J. H. Cheng, X. F. Ma, X. G. Zhou and J. J. Chruma, *Chem. Soc. Rev.*, 2013, **42**, 6128–6185.
8 K. Li, G. S. M. Tong, Q. Wan, G. Cheng, W. Y. Tong, W. H. Ang, W. L. Kwong and C. M. Che, *Chem. Sci.*, 2016, **7**, 1653–1673.
9 S. Campagna, F. Puntoriero and F. Nastasi, *Top. Curr. Chem.*, 2007, **280**, 117–214.
10 Y. Chi and P. T. Chou, *Chem. Soc. Rev.*, 2007, **36**, 1421–1431.
11 L. Flamigni, A. Barbieri, C. Sabatini, B. Ventura and F. Barigelletti, *Top. Curr. Chem.*, 2007, **281**, 143–203.
12 Y. You and S. Y. Park, *Dalton Trans.*, 2009, 1267–1282.
13 A. Y. Y. Tam and V. W. W. Yam, *Chem. Soc. Rev.*, 2013, **42**, 1540–1567.
14 V. W. W. Yam, V. K. M. Au and S. Y. L. Leung, *Chem. Rev.*, 2015, **115**, 7589–7728.
15 X. F. Ma, R. Sun, J. H. Cheng, J. Y. Liu, F. Gou, H. F. Xiang and X. G. Zhou, *J. Chem. Educ.*, 2016, **93**, 345–350.
16 J. Luo, Z. Xie, J. W. Y. Lam, L. Cheng, H. Chen, C. Qiu, H. S. Kwok, X. Zhan, Y. Liu, D. Zhu and B. Z. Tang, *Chem. Commun.*, 2001, 1740–1741.
17 Y. Hong, J. W. Y. Lam and B. Z. Tang, *Chem. Soc. Rev.*, 2011, **40**, 5361–5388.
18 J. Mei, N. L. C. Leung, R. T. K. Kwok, J. W. Y. Lam and B. Z. Tang, *Chem. Rev.*, 2015, **115**, 11718–11940.
19 L. Ravotto and P. Ceroni, *Coord. Chem. Rev.*, 2017, **346**, 62–76.
20 K. Saito, Y. Hamada, H. Takahashi, T. Koshiyama and M. Kato, *Jpn. J. Appl. Phys., Part 2*, 2005, **44**, L500.
21 B. Ma, J. Li, P. I. Djurovich, M. Yousufuddin, R. Bau and M. E. Thompson, *J. Am. Chem. Soc.*, 2005, **127**, 28–29.
22 B. Ma, P. I. Djurovich, S. Garon, B. Alleyne and M. E. Thompson, *Adv. Funct. Mater.*, 2006, **16**, 2438–2446.
23 A. A. Rachford and F. N. Castellano, *Inorg. Chem.*, 2009, **48**, 10865–10867.
24 S. Jamali, R. Czerwieniec, R. Kia, Z. Jamshidi and M. Zabel, *Dalton Trans.*, 2011, **40**, 9123–9130.
25 S. W. Lai, M. C. W. Chan, T. C. Cheung, S. M. Peng and C. M. Che, *Inorg. Chem.*, 1999, **38**, 4046–4055.
26 W. Lu, M. C. W. Chan, N. Zhu, C. M. Che, C. Li and Z. Hui, *J. Am. Chem. Soc.*, 2004, **126**, 7639–7651.
27 C. K. Koo, B. Lam, S. K. Leung, M. H. W. Lam and W. Y. A. Wong, *J. Am. Chem. Soc.*, 2006, **128**, 16434–16435.
28 K. W. Wang, J. L. Chen, Y. M. Cheng, M. W. Chung, C. C. Hsieh, G. H. Lee, P. T. Chou, K. Chen and Y. Chi, *Inorg. Chem.*, 2010, **49**, 1372–1383.
29 R. P. L. Tang, K. M. C. Wong, N. Zhu and V. W. W. Yam, *Dalton Trans.*, 2009, 3911–3922.
30 H. Leopold, M. Tenne, A. Tronnier, S. Metz, I. Mgnster, G. Wagenblast and T. Strassner, *Angew. Chem., Int. Ed.*, 2016, **55**, 15779–15782.
31 P. Pinter, Y. Unger and T. Strassner, *ChemPhotoChem*, 2017, **1**, 113–115.
32 L. Zhou, P. Y. Cai, Y. Feng, J. H. Cheng, H. F. Xiang, J. Liu, D. Wu and X. G. Zhou, *Anal. Chim. Acta*, 2012, **735**, 96–106.
33 X. F. Ma, J. H. Cheng, J. Y. Liu, X. G. Zhou and H. F. Xiang, *New J. Chem.*, 2015, **39**, 492.
34 J. H. Cheng, K. Y. Wei, X. F. Ma, X. G. Zhou and H. F. Xiang, *J. Phys. Chem. C*, 2013, **117**, 16552–16563.
35 J. H. Cheng, Y. H. Zhang, X. F. Ma, X. G. Zhou and H. F. Xiang, *Chem. Commun.*, 2013, **49**, 11791–11793.
36 J. H. Cheng, Y. X. Li, R. Sun, J. Y. Liu, F. Gou, X. G. Zhou, H. F. Xiang and J. Liu, *J. Mater. Chem. C*, 2015, **3**, 11099–11110.
37 X. H. Zhang, J. Shi, G. Y. Shen, F. Gou, J. H. Cheng, X. G. Zhou and H. F. Xiang, *Mater. Chem. Front.*, 2017, **1**, 1041–1050.
38 G. Y. Shen, F. Gou, J. H. Cheng, X. H. Zhang, X. G. Zhou and H. F. Xiang, *RSC Adv.*, 2017, **7**, 40640–40649.
39 J. H. Cheng, X. F. Ma, Y. H. Zhang, J. Y. Liu, X. G. Zhou and H. F. Xiang, *Inorg. Chem.*, 2014, **53**, 3210–3219.
40 J. H. Cheng, F. Gou, X. H. Zhang, G. Y. Shen, X. G. Zhou and H. F. Xiang, *Inorg. Chem.*, 2016, **55**, 9221–9229.
41 D. A. Atwood and M. J. Harvey, *Chem. Rev.*, 2001, **101**, 37–52.
42 P. G. Cozzi, *Chem. Soc. Rev.*, 2004, **33**, 410–421.
43 E. Lamour, S. Routier, J. L. Bernier, J. P. Catteau, C. Bailly and H. Vezin, *J. Am. Chem. Soc.*, 1999, **121**, 1862–1869.
44 P. Wu, D. L. Ma, C. H. Leung, S. C. Yan, N. Y. Zhu, R. Abagyan and C. M. Che, *Chem. – Eur. J.*, 2009, **15**, 13008–13021.
45 H. Miyasaka, A. Saitoh and S. Abe, *Coord. Chem. Rev.*, 2007, **251**, 2622–2664.
46 M. Andruh, *Chem. Commun.*, 2011, **47**, 3025–3042.
47 S. J. Wezenberg, E. C. Escudero-Adán, J. Benet-Buchholz and A. W. Kleij, *Chem. – Eur. J.*, 2009, **15**, 5695–5700.
48 G. Consiglio, S. Failla, P. Finocchiaro, I. P. Oliveri, R. Purrello and S. Di Bella, *Inorg. Chem.*, 2010, **49**, 5134–5142.

49 Y. Hai, J. J. Chen, P. Zhao, H. Lv, Y. Yu, P. Xu and J. L. Zhang, *Chem. Commun.*, 2011, **47**, 2435–2437.
50 H. Y. Yin, J. Tang and J. L. Zhang, *Eur. J. Inorg. Chem.*, 2017, 5085–5093.
51 P. F. Wang, Z. R. Hong, Z. Y. Xie, S. W. Tong, O. Y. Wong, C. S. Lee, N. B. Wong, L. S. Hung and S. T. Lee, *Chem. Commun.*, 2003, 1664–1665.
52 C. M. Che, S. C. Chan, H. F. Xiang, M. C. W. Chan, Y. Liu and Y. Wang, *Chem. Commun.*, 2004, 1484–1845.
53 H. F. Xiang, S. C. Chan, K. K. Y. Wu, C. M. Che and P. T. Lai, *Chem. Commun.*, 2005, 1408–1410.
54 C. M. Che, C. C. Kwok, S. W. Lai, A. F. Rausch, W. J. Finkenzeller, N. Y. Zhu and H. Yersin, *Chem. – Eur. J.*, 2010, **16**, 233–247.
55 J. Zhang, F. C. Zhao, X. J. Zhu, W. K. Wong, D. G. Ma and W. Y. Wong, *J. Mater. Chem.*, 2012, **22**, 16448–16457.
56 N. Komiya, T. Muraoka, M. Iida, M. Miyanaga, K. Takahashi and T. Naota, *J. Am. Chem. Soc.*, 2011, **133**, 16054–16061.
57 S. J. Liu, H. B. Sun, Y. Ma, S. G. Ye, X. M. Liu, X. H. Zhou, X. Mou, L. H. Wang, Q. Zhao and W. Huang, *J. Mater. Chem.*, 2012, **22**, 22167–22173.
58 F. Gou, J. H. Cheng, X. H. Zhang, G. Y. Shen, X. G. Zhou and H. F. Xiang, *Eur. J. Inorg. Chem.*, 2016, 4862–4866.
59 J. Brooks, Y. Babayan, S. Lamansky, P. I. Djurovich, I. Tsyba, R. Bau and M. E. Thompson, *Inorg. Chem.*, 2002, **41**, 3055–3066.
60 L. Pu, *Chem. Rev.*, 2004, **104**, 1687–1716.
61 L. Pu, *Acc. Chem. Res.*, 2017, **50**, 1032–1040.
62 E. M. Sanchez-Carnerero, A. R. Agarrabeitia, F. Moreno, B. L. Maroto, G. Muller, M. J. Ortiz and S. de la Moya, *Chem.–Eur. J.*, 2015, **21**, 13488–13500.
63 J. T. Song, M. Wang, X. G. Zhou and H. F. Xiang, *Chem. – Eur. J.*, 2018, **24**, 7128–7132.
64 C. Garino, A. Erenzi, G. Barone and L. Salassa, *J. Chem. Educ.*, 2016, **93**, 292–298.
65 J. S. Ni, H. X. Liu, J. K. Liu, M. J. Jiang, Z. Zhao, Y. C. Chen, R. T. K. Kwok, J. W. Y. Lam, Q. Peng and B. Z. Tang, *Mater. Chem. Front.*, 2018, **2**, 1498–1507.
66 G. X. Huang, R. S. Wen, Z. M. Wang, B. S. Li and B. Z. Tang, *Mater. Chem. Front.*, 2018, **2**, 1884–1892.
67 H. Nie, K. Hu, Y. J. Cai, Q. Peng, Z. J. Zhao, R. R. Hu, J. W. Chen, S. J. Su, A. J. Qin and B. Z. Tang, *Mater. Chem. Front.*, 2017, **1**, 1125–1129.
68 M. Yamaguchi, S. Ito, A. Hirose, K. Tanaka and Y. Chujo, *Mater. Chem. Front.*, 2017, **1**, 1573–1579.
69 M. Wang, C. Cheng, J. T. Song, J. Wang, X. G. Zhou, H. F. Xiang and J. Liu, *Chin. J. Chem.*, 2018, **36**, 698–707.
70 E. V. Puttock, M. T. Walden and J. A. G. Williams, *Coord. Chem. Rev.*, 2018, **367**, 127–162.
71 G. Z. Lu, Y. M. Jing, H. B. Han, Y. L. Fang and Y. X. Zheng, *Organometallics*, 2017, **36**, 448–454.
72 Y. Tao, K. Yuan, T. Chen, P. Xu, H. H. Li, R. F. Chen, C. Zheng, L. Zhang and W. Huang, *Adv. Mater.*, 2014, **26**, 7931–7958.
73 Z. Y. Yang, Z. Mao, Z. L. Xie, Y. Zhang, S. W. Liu, J. Zhao, J. R. Xu, Z. G. Chi and M. P. Aldred, *Chem. Soc. Rev.*, 2017, **46**, 915–1016.
74 M. Y. Wong and E. Zysman-Colman, *Adv. Mater.*, 2017, **29**, 1605444.

